ADVANCED FUNCTIONAL MATERIALS
www.afm-journal.de

Spin-Crossover Grafted Monolayer of a Co(II) Terpyridine Derivative Functionalized with Carboxylic Acid Groups

Víctor García-López, Niccolò Giaconi, Lorenzo Poggini, Joaquín Calbo, Amélie Juhin, Brunetto Cortigiani, Javier Herrero-Martín, Enrique Ortí, Matteo Mannini, Miguel Clemente-León,* and Eugenio Coronado*

The synthesis and characterization of a new Co(II) spin-crossover (SCO) complex based on 4′-(4-carboxyphenyl)—2,2′:6′,2″-terpyridine ligand are reported. This complex can be successfully grafted on silver surface maintaining the SCO behavior. Thus, atomic force microscopy (AFM), matrix assisted laser desorption ionization – time-of-flight mass spectrometry (MALDI-TOF MS), Raman spectroscopy, and XPS measurements, upon surface deposition, evidence the formation of a monolayer of intact molecules grafted through carboxylate groups to the Ag surface. Three different techniques: Raman spectroscopy, X-ray photoelectron spectroscopy (XPS), and X-ray absorption spectroscopy (XAS), supported by first-principles calculations, confirm that the deposited molecules undergo a gradual spin transition with temperature. This phenomenon is unprecedented for a monolayer of molecules directly grafted onto a metallic surface from solution.

1. Introduction

The integration of magnetic switchable molecular materials in electronic devices has recently aroused great interest in the scientific community.[1,2] In this regard, spin-crossover (SCO) complexes showing magnetic bistability, also at room temperature,[3–6] represent one of the most spectacular examples of magnetic bistability since both low-spin (LS) and high-spin (HS) states are reachable through external stimuli such as temperature, pressure, or light.[7,8] Deposition of these complexes on solid surfaces is a mandatory step for applications such as electrical switches[9–17] or mechanical actuators.[18–23] Over the past 10 years, the preferred method for depositing this type of systems has been sublimation in ultrahigh vacuum (UHV) of neutral complexes.[24–29] Indeed, it has been proven that some nanostructured assemblies of SCO systems achieved in UHV can maintain their switching behavior even down to the sub-monolayer and single-molecule regime.[30–33] However, this deposition method is restricted to a few families of vacuum evaporable molecules.[34]

An interesting alternative to extend the versatility of SCO is the deposition of properly functionalized molecules from solution to afford grafted monolayers. This approach remains almost unexplored, excluding some earlier reports regarding chemisorption of such molecules in a junction-like gold nanoparticle array.[35] This soft and cost-effective deposition method is a general simple grafting method that only requires molecules (neutral or charged) functionalized with suitable anchoring groups able to interact with the

V. García-López, J. Calbo, E. Ortí, M. Clemente-León, E. Coronado
Instituto de Ciencia Molecular
Universidad de Valencia
Catedrático José Beltrán 2, 46980 Paterna, Spain
E-mail: miguel.clemente@uv.es

V. García-López, N. Giaconi, B. Cortigiani, M. Mannini
Department of Chemistry "Ugo Schiff" and INSTM Research Unit
University of Florence
Via della Lastruccia 3–13, 50019 Sesto Fiorentino, Italy
E-mail: matteo.mannini@unifi.it

The ORCID identification number(s) for the author(s) of this article can be found under https://doi.org/10.1002/adfm.202300351

DOI: 10.1002/adfm.202300351

L. Poggini
Istituto di Chimica dei Composti Organometallici (ICCOM)
CNR Via Madonna del Piano, 10, 50019 Sesto Fiorentino, Italy

A. Juhin
Institut de Minéralogie
de Physique des Matériaux et de Cosmochimie (IMPMC)
UMR7590
CNRS
Sorbonne Université
MNHN
4 Place Jussieu, Cedex 5, 75252 Paris, France

J. Herrero-Martín
ALBA Synchrotron
Carrer de la Llum 2–26, Cerdanyola del Vallès, 08290 Barcelona, Spain

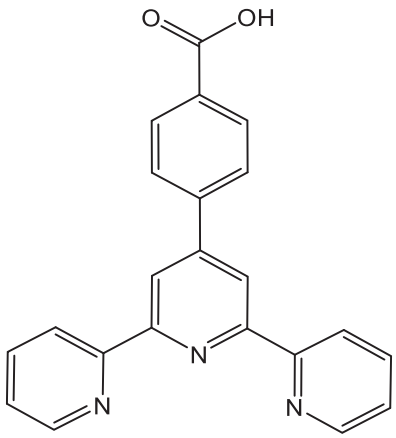

HL

Figure 1. Molecular structure of the ligand 4′-(4-carboxyphenyl)−2,2′:6′,2″-terpyridine, HL.

surface.[36] Previous attempts of the deposition of the homoleptic $[Fe^{II}(L)_2]^{2+}$ (L = 4-(mercapto)−2,6-di(pyrazol-1-yl)pyridine or 4-(*N*-thiomorpholinyl)−2,6-di(pyrazol-1-yl)pyridine)[37] and heteroleptic $[Fe^{II}(bppCOOH)(L')]^{2+}$ (L′ = 2,6-bis(5-([1,1′-biphenyl]−4-yl)−1*H*-pyrazol-3-yl)pyridine or ethyl 2,6-bis(1*H*-pyrazol-1-yl)isonicotinate)[38] and $[Fe^{II}(H_2Bpz_2)_2(L)]$ (H_2Bpz_2=dihydrobis(1-pyrazolyl)-borate, L=tetrathiafulvalene-fused dipyrido-[3,2-a:2,3-c] phenazine)[39] SCO systems failed because of the redox instability of the tested molecules. Here we report that the complex $[Co^{II}(HL)_2]^{2+}$ (**HL** = 4′-(4-carboxyphenyl)−2,2′:6′,2″-terpyridine) can be successfully grafted on silver surfaces maintaining the SCO behavior. The Co(II) complexes adopted in this work have been preferred owing to their robustness against oxidation compared to the Fe(II)-based complexes.[38]

Spin transition in six-coordinated Co(II) compounds (d^7) involves a spin conversion from a S = 1/2 ($t_{2g}^6 e_g^1$) LS state to a S = 3/2 ($t_{2g}^5 e_g^2$) HS state. Many bis-chelated Co(II) SCO complexes incorporating tridentate ligands based on 2,2′:6′,2″-terpyridine (hereafter *terpy*) derivatives have been reported.[40] Among them, those containing substituents at the C(4′) position are of special interest.[41] Indeed, it has been shown that different substituents allow diverse magnetic properties, ranging from abrupt spin transitions to unique SCO behaviors such as reverse spin transitions.[42] Furthermore, the use of specific substituents has enabled to combine SCO with other properties such as porosity,[43] liquid crystal behavior,[44–47] ferroelectricity,[48] or gas sensing.[49] In this work, we have taken profit of this ability to carry additional features while maintaining SCO by using a Co(II) complex incorporating **HL**, a *terpy* derivative with a carboxylic acid group,[50] see **Figure 1**. Hereby, we intend to take advantage of the anchoring capabilities of the carboxylic acid group on silver to form grafted monolayers from solution at room temperature of a Co(II) SCO complex.[51,52]

The structure of the Co(II) neutral complex with the deprotonated ligand **L**, $[Co(L)_2]\cdot 5H_2O$, was reported in the literature by Yang et al.,[53] but the magnetic properties were not studied. Thus, we also prepared the complex with the protonated ligands $[Co(HL)_2](ClO_4)_2\cdot 4DMA$ (**1**, DMA=dimethylacetamide), which has been structurally and magnetically characterized in the solid state, in order to optimize its processability, and we studied its behavior upon surface deposition. The morphology, stability, and composition of deposited monolayers of 1 on top of Ag (1/Ag) were studied by atomic force microscopy (AFM), matrix assisted laser desorption ionization – time-of-flight mass spectrometry (MALDI-TOF MS), X-ray photoelectron spectroscopy (XPS), and Raman spectroscopy. SCO properties were further investigated by means of XPS, Raman, and X-ray absorption spectroscopy (XAS), assisted by first-principles calculations, which confirm that the spin state of the Co(II) complexes on top of Ag displays gradual and reversible changes with temperature.

2. Results and Discussion

2.1. Solid State

2.1.1. Synthesis

Complex 1 was obtained by slow diffusion of diethyl ether into solutions of $Co(ClO_4)_2\cdot xH_2O$ and **HL** in a 1:2 molar ratio in DMA. After a few weeks, big prismatic dark-orange crystals suitable for single-crystal diffraction were obtained. Purity and stability of the complex were checked with elemental analysis and powder X-ray diffraction (Figure S1, Supporting Information).

2.1.2. Structure

The crystal structure of 1 was solved by single-crystal X-ray diffraction at 120, 300, and 340 K in the centrosymmetric *P*-1 space group. The asymmetric unit is composed of one $[Co(HL)_2]^{2+}$ cation, two ClO_4^- anions, and four DMA solvent molecules (**Figure 2**a and Supporting Information for more information). The metal center is coordinated to the six nitrogen atoms of the two terpyridine moieties giving rise to a distorted octahedral geometry. Co–N bonds display a subtle increase in length with temperature (see Table S1, Supporting information). This indicates that the number of molecules in the HS state increases with temperature, as it has been already observed in other compounds,[7] and agrees with the evolution of the magnetic properties with temperature (see below). Neighboring $[Co(HL)_2]^{2+}$ cations in the structure are weakly interacting through $\pi\cdots\pi$ and CH$\cdots\pi$ interactions (see Figure S2, Supporting Information), while hydrogen bonds with the DMA solvent molecules avoid the formation of 1D chains of hydrogen-bonded $[Co(HL)_2]^{2+}$ cations (see Figure 2a), which are found in other bis-tridentate 4-substituted pyridine derivatives.[54,55]

2.1.3. Magnetic Properties

The temperature dependence of $\chi_M T$ for 1 in contact with mother liquor presents a gradual increase from typical LS values below 150 K (0.48 cm^3 K mol^{-1}) to 1.85 cm^3 K mol^{-1} at 350 K with a thermal SCO temperature $T_{1/2}$ ($T_{1/2}$=temperature of 50% HS to LS conversion) of ≈280 K considering 0.5 and 2.5 cm^3 K mol^{-1} as approximate LS and HS values, respectively. [42] This suggests an

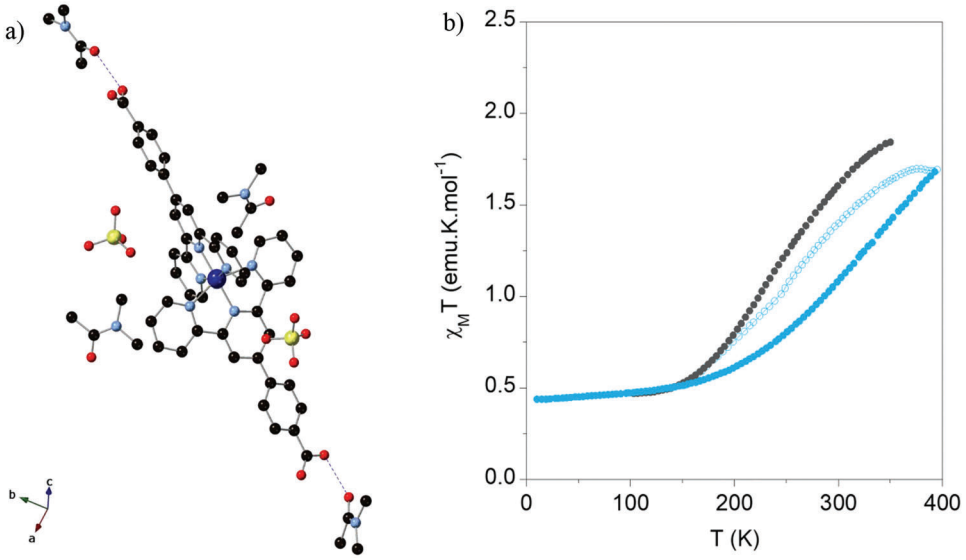

Figure 2. a) X-ray single-crystal structure of complex 1 at 120 K. C (black), N (blue), O (red), Co (dark blue), and Cl (yellow). Hydrogen atoms are omitted for clarity and hydrogen bonds are represented with dashed blue lines. b) $\chi_M T$ versus temperature for 1 in contact with mother liquor (grey circles), filtered (blue empty circles), and after complete desolvation (filled blue circles).

incomplete and non-cooperative spin transition (Figure 2b). Magnetic measurements on the filtered sample before and after heating up to 400 K show a similar behavior, with a more incomplete SCO transition reaching a maximum value of 1.72 cm^3 K mol^{-1} at 400 K. This value corresponds to ≈60% of molecules in the HS state, considering 2.5 cm^3 K mol^{-1} as the value for pure Co(II) in HS state.

In contrast, the Co(II) neutral complex with the deprotonated ligand **L**, $[Co(L)_2]\cdot 5H_2O$, shows an abrupt thermal spin transition upon dehydration (see associated text and Figure S3, Supporting Information). This suggests that the gradual spin transition in 1 may be due to the presence of ClO_4^- counterions and DMA solvent molecules in the structure, which leads to the absence of strong intermolecular interactions. At variance, the absence of solvent molecules in the dehydrated $[Co(L)_2]$ compound would involve closer contacts between complexes leading to a cooperative and abrupt SCO. A similar effect occurs in the Co(II) SCO complex based on the terpyridine derivative without the phenyl spacer between the *terpy* and the carboxylic acid: [49] the more compact structure obtained upon dehydration leads to a more abrupt SCO.

2.2. Deposition

2.2.1. Monolayer Preparation

1/Ag and L/Ag were prepared by immersing evaporated silver substrates, treated with hydrogen flame-annealing (see Supporting Information for further details), for 6 h in a 1 mM anhydrous DMA solution of 1 and L, respectively. After that, they were washed and rinsed thoroughly with clean DMA to remove any physisorbed material and dried under N_2 stream. Silver was chosen as substrate with the aim of promoting chemisorption of both molecules through the interaction with carboxylate moieties,[52] which may form large domains of well-ordered 2D molecular arrays at room temperature within a short time promoted through this kind of interaction.[51]

2.2.2. Atomic Force Microscopy (AFM)

AFM provides information about the homogeneity of the surface because, when the formed monolayer replicates the topography of the underlaying surface, AFM experiments in air tapping mode lack the resolution to provide a direct proof of the formation of an ordered monolayer. However, topographic images of 1/Ag and L/Ag confirmed the absence of big aggregates or multilayers (see Figure S4, Supporting Information). This result was expected considering that the carboxylate group bonds selectively the silver surface, and in case, additional physisorbed layers can be easily removed with the washing steps.

2.2.3. Matrix Assisted Laser Desorption Ionization – Time-of-Flight Mass Spectrometry (MALDI-TOF MS)

Integrity of the molecules in 1/Ag was checked with MALDI-TOF MS. A comparative analysis between bulk and monolayer is shown in **Figure 3**. Peaks of *m/z* corresponding to $[Co(HL)_2]^+$ are present in both spectra (764.16 *m/z*). Proof of the formation of a bond between only one carboxylate group of the molecules and the surface is supported by the presence of signals originated from a silver atom that is extracted together with molecular fragments such as $[L+H+Ag]^+$, $[Co(HL+H+Na)(L+Ag)]^+$, and $[Co(HL\text{-}COOH+H)(L+Ag)]^+$; these signals are not present in the bulk sample (Figure 3). This result has been reported previously in other systems grafted on Au,[56–58] where a molecule-substrate bonding is expected and suggests that deprotonation of the carboxylic acid group takes place upon contact with the

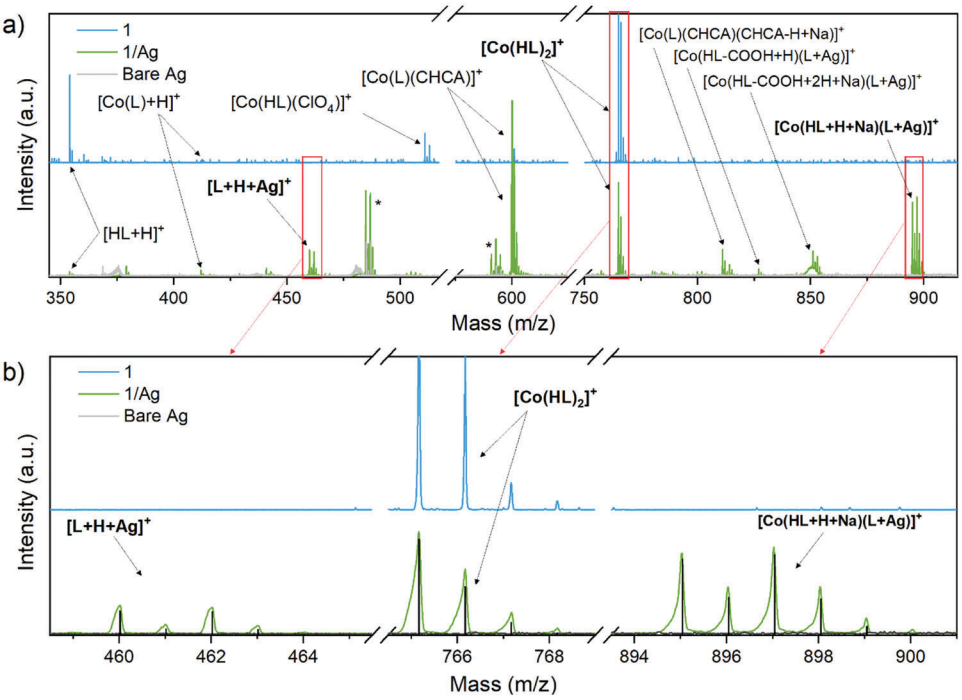

Figure 3. a) MALDI-TOF MS spectra of **1** (blue), **1/Ag** (green), and bare Ag (grey). b) Magnification of the $[L + H + Ag]^+$, $[Co(HL)_2]^+$, and $[Co(HL + H + Na)(L + Ag)]^+$ (enclosed in red rectangles). The expected isotopic distribution pattern for each fragment is reported as black lines. Peaks coming from the matrix used for calibration are marked with an asterisk and are also observed in bare Ag. CHCA is abbreviation for α-cyano-4-hydroxycinnamic acid, and it is present in the matrix used for MALDI-TOF MS measurements (see Experimental Section).

surface. Additionally, the lack of molecular fragments in the monolayer sample with the counter-anion, such as $[Co(HL)(ClO_4)]^+$, that are present in the bulk sample, also confirms the absence of aggregates or any physisorbed multilayers in agreement with AFM measurements (for further information see Table S3, Supporting Information).

2.2.4. Monolayer Modeling

Theoretical calculations at the cost-effective GFN2-xTB level of theory[59,60] were performed to shed light on the orientation and organization of the Co(II) SCO molecules on the Ag surface. First, two molecules of **1** were placed onto a Ag surface in a range of intermolecular distances that varied from 6 to 14 Å, and the geometries were relaxed by keeping fixed the anchor-anchor distance (d_{AA}; **Figure 4**a). A binding energy (E_{bind}) of 3–4 kcal mol^{-1} is predicted for d_{AA} between 8 and 13 Å, being the largest E_{bind} of −3.80 kcal mol^{-1} for 10.5 Å (Figure S5, Supporting Information). This net stabilization mainly arises from π–π (3.2–3.4 Å) and CH···π (2.6–2.9 Å) contacts between the aromatic pyridine cores of neighboring molecules. Non-covalent interactions (NCI) surfaces [61] confirm the presence of these weak but attractive forces (Figure 4a,b). Note that E_{bind} is relatively small, and interaction with solvent media at room temperature may compensate the complex–complex intermolecular stabilization. By replicating the minimum-energy supramolecular dimer (d_{AA} = 10.5 Å), a four-complex assembly was modeled, which upon optimization led to a E_{bind} of −6.33 kcal mol^{-1}, almost double of that calculated for the dimeric model (see Figure S6, Supporting Information for the minimum-energy structure and Figure S7, Supporting Information for the NCI surfaces). A schematic model of the Co(II) SCO monolayer is depicted in Figure 4c.

2.2.5. Raman Spectroscopy and SERS

Molecular deposits on top of a mechanically roughened silver substrate were characterized by performing Raman spectroscopy. This was possible because of the nature of the imposed silver defects and their small separation that led to a plasmon absorbance, which is resonant with the 532 nm light used to excite the samples.[62] Therefore, the Raman spectrum of the deposits is expected to be magnified in the "hot-spots" by the Surface-Enhanced Raman Scattering (SERS) effect.[63] The structural integrity of the molecules in 1/Ag is evident from the fact that SERS spectra of the monolayer and conventional Raman spectra of the bulk are found to be very similar (see **Figure 5**).

The most important difference between both samples was the replacement of the band at 783 cm^{-1} in the bulk with another one at 814 cm^{-1} in the monolayer. This band is assigned to the deformation vibration of carboxylate groups and it is sensitive to the protonation/deprotonation state.[64] Density functional theory (DFT) calculations on a model system of benzoic acid (see the Supporting Information for computational details) confirm a shift to higher wavenumbers of the Raman intense scissoring mode of COO^- upon deprotonation (from 749 to 793 cm^{-1}, Table S4 and Figure S8, Supporting Information), in line with

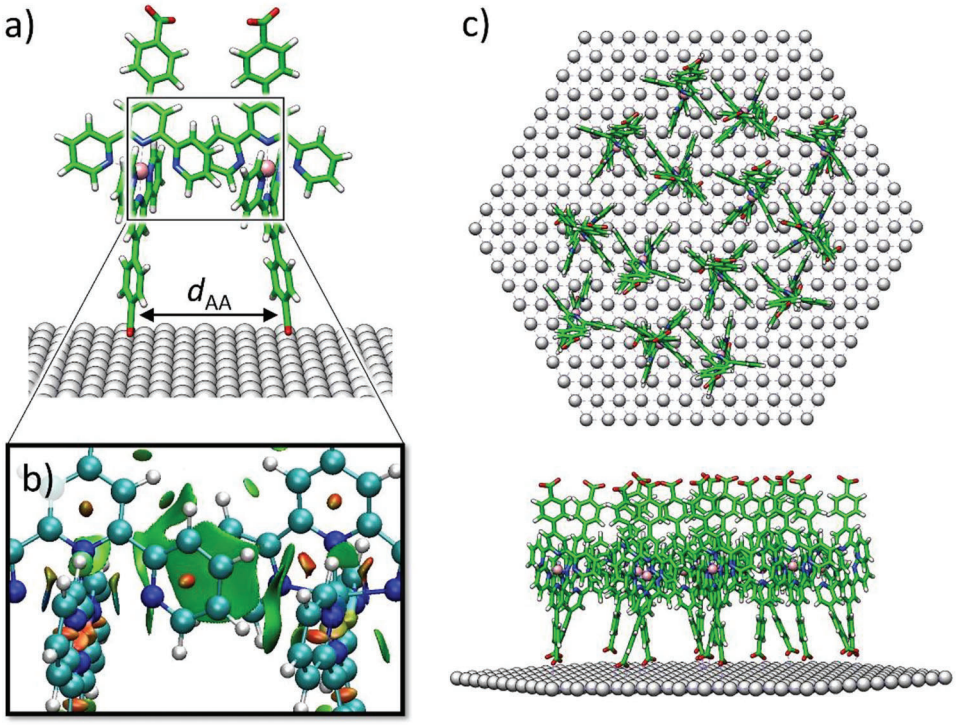

Figure 4. a) Minimum-energy structure calculated for the most stable Co(II) SCO complex dimer at a fixed anchor-anchor distance (d_{AA}) of 10.5 Å using the GFN2-xTB method. b) Inset displaying the NCI surfaces for the π–π and CH··· π interactions that stabilize the supramolecular SCO complex dimer. c) Top and side views of a schematic model of the Co(II) SCO monolayer.

that reported in the literature.[64,65] Such band was also present in the spectra of the complex $[Co(L)_2]\cdot 5H_2O$[53] (Figure 5) and in the spectra of the monolayer of the ligand (L/Ag, see Figure S9, Supporting Information), both measured as references. Deprotonation of the carboxylic acid group in contact with the surface was expected, as it has been already observed in literature experiments performed with similar ligands on Ag.[52] On the other hand, knowing the protonated/deprotonated state of the carboxylic acid group non-interacting with the surface is not straightforward. However, the presence of only one band indicates that both carboxylic acid groups of the deposited complexes are deprotonated,[66] which is indeed consistent with the absence of ClO_4^- counter-anions observed in the XPS experiments performed on 1/Ag (see below), and, therefore, compensates the +2 charge of the complexes. To support this conclusion, theoretical calculations were performed on 1, deprotonated 1 ($[Co(L)_2]$), and deprotonated 1 bound to a simplified model of a silver cluster to simulate 1/Ag (see the Supporting Information for details). Frequency analysis confirms the presence of a COO^- scissoring mode (coupled with phenyl C–H rocking) at 785 and 797 cm^{-1} for $[Co(L)_2]$ and 1/Ag, respectively (see Figure S10, Supporting Information), which are shifted to higher wavenumbers compared to **1** (744 cm^{-1}), in good accord with the trends found in Raman experiments (Figure 5).

Additionally, temperature dependent Raman spectroscopy experiments were used to monitor the spin state variation of the

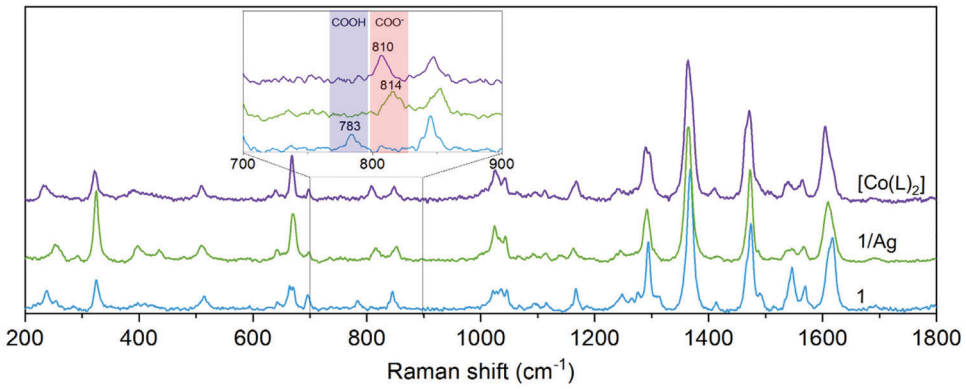

Figure 5. Raman spectra of **1** (blue), **1/Ag** (green), and $[Co(L)_2]\cdot 5H_2O$ (purple) in the 200–1800 cm^{-1} at 100K. Inset of the 700–900 cm^{-1} region.

Co(II). In the bulk sample, changes in intensity ratios and Raman shifts were observed in the same temperature range of the spin transition, especially in the coordinative *terpy* modes (1200–1700 cm^{-1}, see Figure S11a, Supporting Information). Nevertheless, the most notable feature was the increase of intensity of the peak located at 1020 cm^{-1} observed when increasing temperature. This peak is assigned to the pyridine ring breathing mode,[67] which is strongly coupled to the Co–N stretching and, in consequence, to the spin state. Similar Raman spectral changes of this peak accompanying spin transition were observed in a related Co(II) complex reported in the literature.[68] DFT simulations of the Raman spectrum of 1 in LS and HS states evidence the main differentiating feature at ≈1000 cm^{-1} (see Figure S12, Supporting Information). A closer inspection on the vibrational modes in that region confirm their nature: breathing modes of the pyridine rings with participation of the N, which is directly connected to Co. While in the LS state several medium-intense vibrations are predicted in the 980–1020 cm^{-1} region (see Figure S13, Supporting Information), a main vibrational mode implying symmetric Co–N stretching of all pyridines, which approximately doubles the intensity of the LS peaks, rises for the HS state at 1001 cm^{-1} (see Figure S14, Supporting Information). This trend, which nicely correlates with the experimental data, may be ascribed to the more symmetric coordination environment found for the HS state, compared to the LS state, as a result of a weaker Jahn–Teller effect (see Figure S15, Supporting Information).

To get a qualitative insight of the HS/LS conversion, the normalized intensity of such feature (integrated against the weak temperature-dependent mode of the 4-substituted position of the pyridine ring at 1365 cm^{-1})[67] is plotted against temperature (Figure S11b, Supporting Information). It displays a gradual increase with temperature, which is in excellent agreement with the bulk data extracted from conventional magnetometry measurements. Therefore, these Raman spectral changes can be attributed to a spin transition and used to monitor the spin state. SERS spectra of 1/Ag display similar changes with temperature (see **Figure 6**a, further intermediate temperatures are reported in Figure S16, Supporting Information). These changes are not observed in L/Ag (see Figure S17, Supporting Information), so we can conclude that these variations of the spectrum are attributable to a temperature dependent SCO behavior of 1/Ag. A comparison of the spin transition of the bulk with that of the monolayers of 1 and **L**, using the same spin state-dependent marker, suggests that 1 and 1/Ag undergo spin transition in the same temperature range (150–300 K), while L/Ag does not display any changes (Figure 6b). The fraction of HS molecules seems to be higher in 1/Ag. These results are confirmed by XPS and XAS measurements, which enable a more accurate estimation of the LS/HS fraction (see below).

To prove stability and reproducibility of the spin transition, after the first set of measurements, the sample was stored in air for 1 week, and two more cooling and warming cycles were performed (Figure 6c,d). They confirm that the spin transition in the monolayer is reversible in the temperature range 100–360 K. Further increase in temperature leads to irreversible changes in the spectra and blocking of the spin state (see Figure S18, Supporting Information). L/Ag exhibits the same irreversible changes (see Figure S19, Supporting Information and associated text), suggesting that the irreversibility of the spin transition at temperatures above 360 K is related to structural changes of the molecules.[69,70] Indeed, the irreversibility of the spin transition when heating the monolayer above 360 K was confirmed by XAS (see below).

2.2.6. X-Ray Photoelectron Spectroscopy

C*1s*, N*1s*, Cl*2p*, and Co*2p* XPS regions were analyzed in parallel for the bulk sample of 1 and for the monolayer deposit 1/Ag (see Figure S20 and Table S5, Supporting Information). Line shape of the C*1s* band features three main components for each sample; two at lower energies at 285.0 and 286.5 eV corresponding to C–C/C=C and C–N/C=N species, respectively;[71] and the third one, assigned to O–C=O carbon atoms,[72] that exhibits a shift from 288.9 to 288.1 eV from the bulk to the monolayer. A lower binding energy is consistent with the presence of carboxylate species in the deposited molecules, and it is also present in L/Ag (see Table S5, Supporting Information). N*1s* regions show only one component at 399.7 eV assigned to the coordinated nitrogen atoms of the pyridine rings for both samples.[73] Cl*2p* spectrum of 1 features the typical shape of the perchlorate anion centered at 208 eV,[74] while 1/Ag does not display such signal (see **Figure 7**). This is further experimental evidence of the absence of physisorbed molecules on the surface and of the deprotonation of the carboxylic acid groups upon deposition. This result agrees with the conclusion drawn from the C*1s* region, MALDI-TOF MS data, and Raman spectroscopy.

The Co$2p_{3/2}$ region of the bulk and monolayer displays the expected line shape of a Co(II) photoemission spectra (see Figure 7).[75,76] In order to get qualitative information about the SCO properties, the Co$2p_{3/2}$ region was fitted with a procedure similar to that previously reported for HS/LS-Co(II), where the intensity of the satellites is directly correlated to the paramagnetism, i.e., to the spin state of the metal ion.[57] The line shapes were reproduced with four Co$2p_{3/2}$ components (A–D) along with the corresponding Co$2p_{1/2}$ spin–orbit (SO) coupled contributions (A′–D′) weighted by the expected 2:1 integral ratio (Figure 7). 1 and 1/Ag Co$2p_{3/2}$ components are composed by a main peak A at 780.4 eV for the bulk and 780.8 eV for the monolayer, integrating ≈ 21.6% and 23.3% of the overall signal at 170 K and 17.8% and 18.1% at 300 K, respectively (for satellite peak positions and contributions see Table S6, Supporting Information). Furthermore, a fifth component (E) appears at low binding energies for both samples at ≈778 eV. With transition elements, the presence of prominent shake-up satellites typically occurs with paramagnetic states and can be relatively intense. Therefore, we attribute this to the characteristic cobalt(II)/(III) $L_3M_{23}M_{45}$ (^1P) valence-type Auger peak with a total contribution of less than 5%.[77] Semiquantitative analysis and elemental stoichiometric ratios of 1 and 1/Ag (Tables S6 and S7, Supporting Information) are in good agreement with the expected values. This suggests that most of the molecules covering the surface retain the molecular structure found in the bulk.

XPS was also used to get an insight on the electron level population and thus of the spin state. On one hand, experimental results[75,78,79] confirm that SO splitting (Δ_{SO}) increases with the number of unpaired 3*d*-electrons, being closer to 15 eV for LS-Co(II) and 16 eV for HS-Co(II) species, respectively. Indeed, a

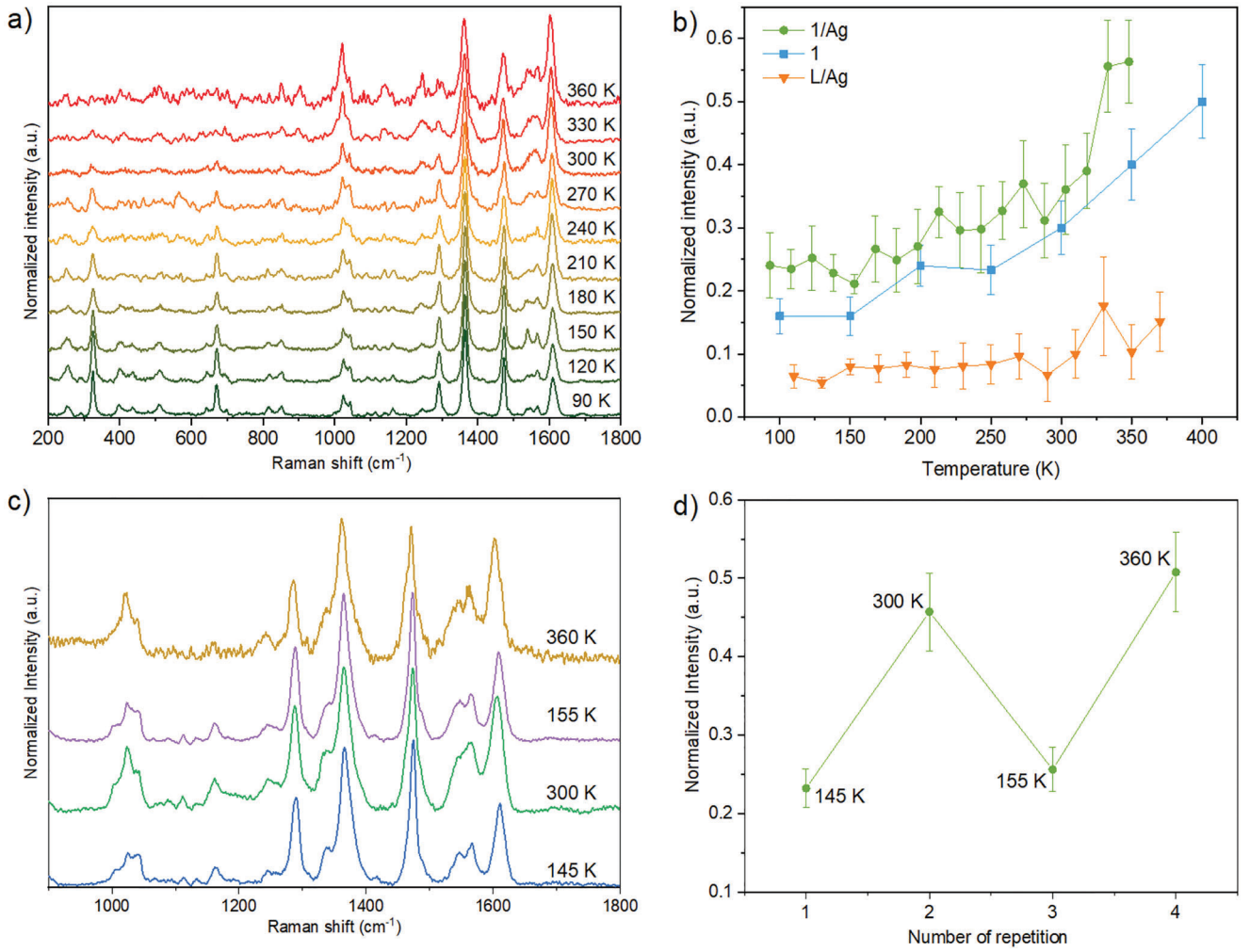

Figure 6. a) Temperature-dependent Raman spectra of **1/Ag** in the 200–1800 cm^{-1} range. b) Normalized intensity of the 1020 cm^{-1} features for **1** (blue squares), **1/Ag** (green circles), and **L/Ag** (orange triangles) for each temperature. c) Temperature-dependent Raman spectra of the same sample after being stored in air for 1 week in the 900–1800 cm^{-1} range. d) Values of the normalized intensity of the 1020 cm^{-1} feature (green circles) at each temperature for the subsequent cooling and warming cycles. The lines are a guide to the eye. Error bars were calculated from the median absolute deviation.

change in Δ_{SO} upon spin transition is expected due to different orbital populations in the two spin states, being larger for HS-Co(II) than for LS-Co(II). Therefore, the occurrence of SCO can be followed by the SO shift.[80] On the other hand, the contribution of the satellites is also indicative of the spin state, an increase in the number of unpaired atomic electrons causes an increase in the satellite intensity in XPS.[57,81] Therefore, the ratio of the integrated area ($\sum I_{sat}/I_{Co\,2p3/2}$) is directly related to the intensity of the satellites and was selected as the most sensitive parameter to follow the spin transition.[75] Co $2p_{3/2}$ XPS region was measured at 170 and 300 K to analyze the differences between low and high temperature species. A slight variation of the Δ_{SO} of ≈0.1 eV was observed in both samples (from 14.9 to 15.0 eV in the bulk and from 15.1 to 15.3 eV in the monolayer) upon increasing the temperature (Table S6, Supporting Information). To confirm the spin transition, together with the high-energy shift of the metal lines, satellite magnification is also expected. Indeed, the increment in $\sum I_{sat}/I_{Co\,2p3/2}$ values (from 1.94 to 2.66 in 1 and from 1.75 to 2.58 in 1/Ag at 170 and 300 K, respectively) indicates that the complexes undergo thermal spin transition, confirming the stability of the SCO properties under X-ray irradiation in UHV.

2.2.7. X-Ray Absorption Spectroscopy

XAS spectra were recorded at Co L_3-edge of 1 and 1/Ag at different temperatures. For the bulk, the spectrum measured at 100 K (see Figure S21a, Supporting Information), according to magnetic properties, is consistent with all Co(II) centers in the LS state, and it is in agreement with the spectra calculated in the Ligand Field Multiplet (LFM) approach for two references of LS-Co(II) in distorted octahedral environment (see Figure S22, Supporting Information), namely Co(II)-imide[82] and Co(II)-phtalocyanine.[83] The spectrum measured at 370 K is not the signature of pure HS-Co(II) but is actually a mixture of HS- and LS-Co(II). A 0.4 fraction of the LS-Co(II) spectrum (i.e., the

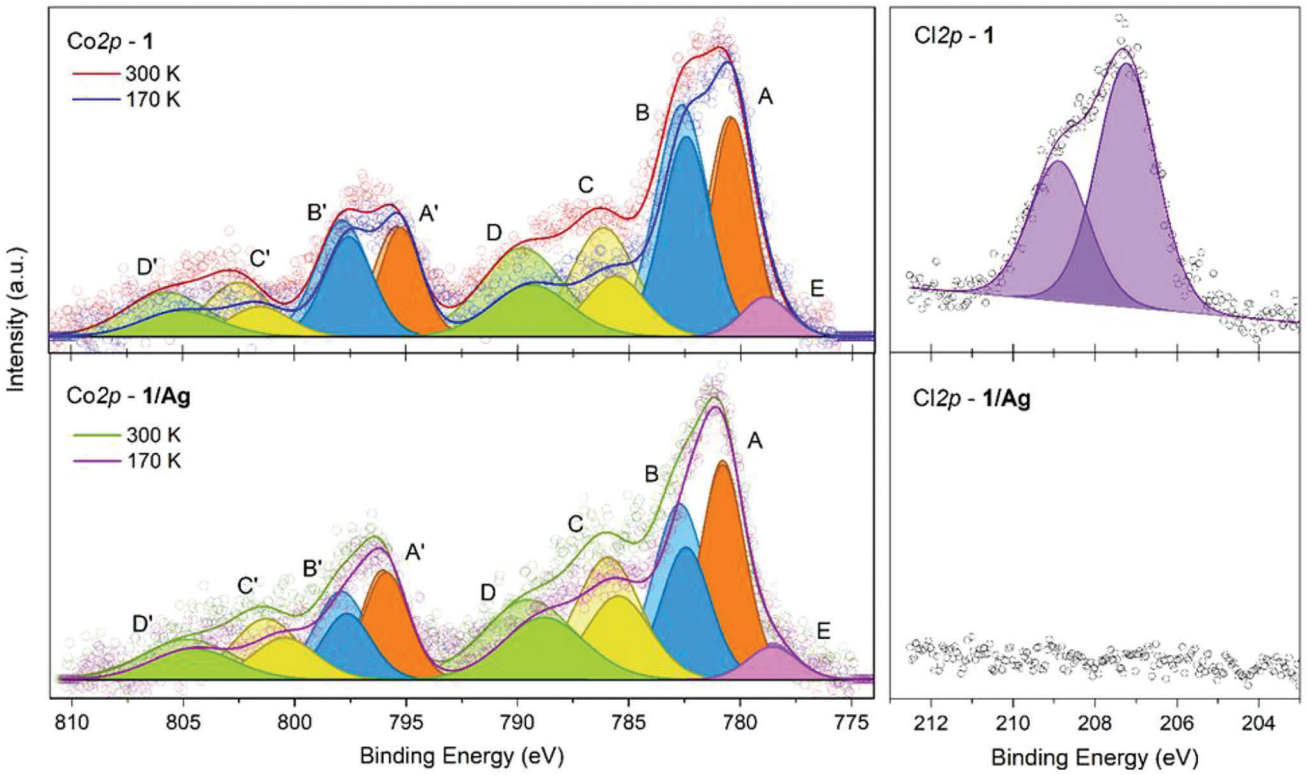

Figure 7. Comparison of XPS Co2*p* and Cl2*p* spectra of **1** (top) and **1/Ag** (bottom) along with deconvolution of the peaks and corresponding best fitting lines.

fraction determined from magnetic measurements) was therefore subtracted, yielding an experimental HS contribution that is consistent with the HS-Co(II) theoretical spectrum (see Figures S21b and S22, Supporting Information) and with previously published data.[84,85] We note a minor fraction (≈3%) of LS octahedral Co(III) (peak at ≈781.4 eV), a feature that increases in sequential scans, so both with time and high photon flux (see Figure S23, Supporting Information). **Figure 8**a shows the temperature-dependent XAS spectra of the monolayer in the 125–310 K range recorded with a minimized photon flux. Evolution of the signal under soft X-ray irradiation was initially excluded at all temperatures (see Figure S24, Supporting Information). However, comparison with the bulk spectra shows a peak at 781.4 eV arising from LS octahedral Co(III) (see Figure S25, Supporting Information) as previously observed for 1. This shows that a fraction of molecules is oxidized either by i) the deposition procedure, ii) the photon damage, or iii) impurities arising from the bulk starting material. The amount of Co(III) will be quantified below using least-squares interpolation (see Table S8, Supporting Information).

To provide a quantitative insight on the temperature-dependence of the Co spin and valence states, the Co L_3 XAS spectra of 1/Ag were fitted using the LFM simulated HS-Co(II) and LS-Co(III) contributions, and the experimental LS-Co(II) spectrum of the bulk (Figures S21 and S22, Supporting Information). The latter was preferred over the LFM simulated LS-Co(II) spectrum because the fine structure is strongly dependent on the crystal field distortion parameters used in the calculation, which are currently unknown for 1/Ag. The results (see Figures S26 and S27, Supporting Information for all the fitted curves) evidence a fraction of oxidized Co(III) molecules, while the rest (Co(II) molecules) undergo a spin transition (see Figure 8b). Two warming cycles were performed to confirm the reversibility of the spin transition in the monolayer (Figure 8b). If we do not consider this Co(III) fraction and normalize the HS-Co(II) contribution to the total (HS+LS) Co(II) contribution, our results indicate that the monolayer features a higher HS content than the bulk for all the temperatures considered, in good agreement with Raman experiments. More precisely, the HS fraction increases from ≈61(3)% to 91(3)% (see Table S9, Supporting Information) for the monolayer and from ≈0% to 30% for the bulk when warming the sample over the working temperature range. These results confirm that the thermal spin transition converts ≈30% of molecules both in the monolayer and bulk samples, but a significant fraction of molecules (≈60%) remain in the HS state at 125 K on the former, which is not the case for the later (≈0%). However, reversibility breaks down when warming 1/Ag at 370 K. The XAS spectrum at 370 K is consistent with the Co(II)-HS state extracted from the bulk, but the subsequent cooling does not affect the spin state and the molecules remain trapped in the HS state (see Figure S28, Supporting Information), in agreement with Raman spectroscopy. These results contrast with previous results of SCO molecules deposited on metallic substrates, such as Au and Cu, which tend to suppress changes in spin state due to the interactions with the substrate that lock spin crossover molecules in a particular or mixed spin state.[86]

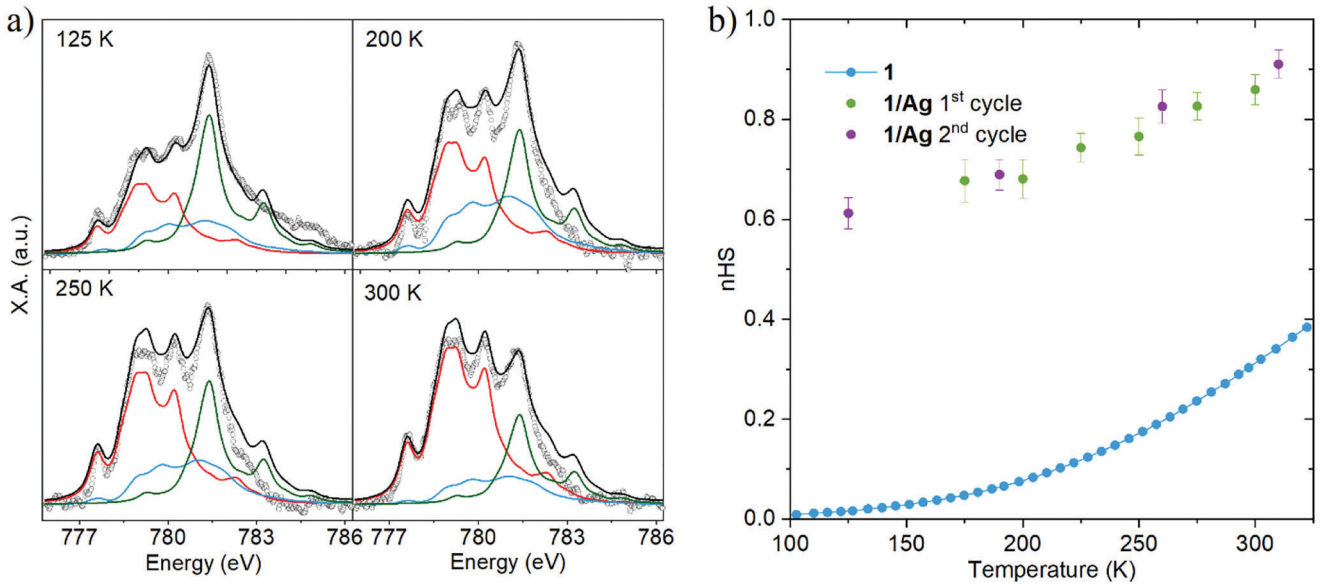

Figure 8. a) XAS Co L_3-edge of **1/Ag** at each temperature (empty circles) together with HS Co(II) (red curves), LS Co(II) (blue curves), and LS Co(III) (green curve) components. Black line is the best fitting curve with the sum of the three components. b) HS Co(II) molar fraction thermal distribution obtained from standard magnetometry on a polycrystalline sample of the bulk (blue dots) and from the XAS regression of **1/Ag** in the first (green dots) and second (purple dots) warming/cooling cycles.

3. Conclusion

Herein, we report the synthesis and characterization of a new Co(II) SCO complex based on 4′-(4-carboxyphenyl)−2,2′:6′,2″-terpyridine ligand. The chemical functionalization of the system provided by the versatile anchoring point and the processability enabled by the higher solubility of the salt allowed us to prepare grafted monolayers of intact molecules from a diluted solution within a short period of time. AFM, MALDI-TOF MS, Raman spectroscopy, and XPS measurements evidence the formation of the deprotonated species upon surface deposition and confirm the absence of physisorbed material. Thermal SCO properties of the monolayer have been confirmed with a set of different techniques: Raman spectroscopy, XPS, XAS, and first-principles calculations, pointing to a gradual SCO behavior. This has also been observed in the solid state for the protonated complex, thus suggesting the absence of a cooperative spin transition on the surface. This represents, as far as we are aware, the first monolayer formed by active SCO complexes anchored to a metallic substrate from solution. Finally, our contribution paves the way to the realization of SCO nanostructure-based devices through soft methodologies compared to the conventional UHV techniques. Further improvements, such as a more abrupt SCO and higher stability, could be achieved by expanding the aromaticity of the ligand to enhance the intermolecular interactions between the deposited molecules.

Supporting Information

Supporting Information is available from the Wiley Online Library or from the author.

Acknowledgements

The authors acknowledge the financial support from the European Union (ERC Advanced Grant MOL-2D 788222 and FET-OPEN SINFONIA 964396), the Spanish MCIN (PID2020-117264GB-I00, PID2020-117152RB-100 and PID2020-119748GA-I00 co-financed by the FEDER and Excellence Unit "María de Maeztu", CEX2019-000919-M), and the Generalitat Valenciana (PROMETEO program, GV/2021/027 and iDiFEDER/2018/061). This study forms part of the Advanced Materials programme and was supported by MCIN with funding from the European Union NextGenerationEU (PRTR-C17.I1) and by Generalitat Valenciana. Proteomic measurements were performed in the proteomics facility of SCSIE University of Valencia. This proteomics laboratory is a member of Proteored. The authors acknowledge the Italian MIUR, through the Project "Dipartimenti di Eccellenza 2018–2022 (ref. no. B96C1700020008) and Fondazione Cassa di Risparmio di Firenze (Project SPINE-2 2020.1634) for the financial support to run experiments at the CeTeCS facilites. The authors thank J. M., Martínez-Agudo, G. Agustí, and A. López-Muñoz from the University of Valencia for their help with magnetic measurements, temperature-variable Raman measurements and XAS measurements, and H. Elnaggar from Sorbonne Université for her help with Quanty. XAS experiments were performed at BL29-BOREAS beamline at ALBA Synchrotron with the collaboration of ALBA staff in both proposal (2020094498) and in-house experiments. The staff of the MatchLab Interdepartmental Research Unit, Università degli Studi di Firenze is also acknowledged.

Conflict of Interest

The authors declare no conflict of interest.

Data Availability Statement

The data that support the findings of this study are available from the corresponding author upon reasonable request.

Keywords

Co(II), grafted monolayers, spin-crossover, X-ray absorption spectroscopy

Received: January 10, 2023
Revised: June 8, 2023
Published online: July 2, 2023

[1] S. Sanvito, *Chem. Soc. Rev.* **2011**, *40*, 3336.
[2] E. Coronado, *Nat. Rev. Mater.* **2019**, *5*, 87.
[3] I. Šalitroš, N. T. Madhu, R. Boča, J. Pavlik, M. Ruben, *Monatsh. Chem.* **2009**, *140*, 695.
[4] B. Schäfer, C. Rajnák, M. Ruben, O. Fuhr, D. Klar, C. Schmitz-Antoniak, H. Wende, M. Ruben, *Chem. Commun.* **2013**, *49*, 10986.
[5] V. García-López, M. Palacios-Corella, S. Cardona-Serra, M. Clemente-León, E. Coronado, *Chem. Commun.* **2019**, 55.
[6] M. Seredyuk, K. Znovjyak, F. J. Valverde-Muñoz, I. da Silva, M. C. Muñoz, Y. S. Moroz, J. A. Real, *J. Am. Chem. Soc.* **2022**, *144*, 14297.
[7] P. Gütlich, H. A. Goodwin, *Spin Crossover in Transition Metal Compounds*, Springer, Berlin, Heidelberg, **2004**.
[8] M. A. Halcrow, *Spin-Crossover Materials: Properties and Applications*, John Wiley & Sons, Ltd., New York, UK **2013**.
[9] J. Dugay, M. Giménez-Marqués, T. Kozlova, H. W. Zandbergen, E. Coronado, H. S. J. van der Zant, *Adv. Mat.* **2015**, *27*, 1288.
[10] A. Holovchenko, J. Dugay, M. Giménez-Marqués, R. Torres-Cavanillas, E. Coronado, H. S. J. van der Zant, *Adv. Mat.* **2016**, *28*, 7228.
[11] J. Dugay, M. Aarts, M. Gimenez-Marqués, T. Kozlova, H. W. Zandbergen, E. Coronado, H. S. J. van der Zant, *Nano Lett.* **2017**, *17*, 186.
[12] L. Poggini, M. Gonidec, J. H. González-Estefan, G. Pecastaings, B. Gobaut, P. Rosa, *Adv. Electron. Mater.* **2018**, *4*, 1800204.
[13] L. Poggini, M. Gonidec, R. K. C. Balasubramanyam, L. Squillantini, G. Pecastaings, A. Caneschi, P. Rosa, *J. Mater. Chem. C* **2019**, *7*, 5343.
[14] R. Torres-Cavanillas, R. Sanchis-Gual, J. Dugay, M. Coronado-Puchau, M. Giménez-Marqués, E. Coronado, *Adv. Mat.* **2019**, *31*, 1970193.
[15] G. Cucinotta, L. Poggini, N. Giaconi, A. Cini, M. Gonidec, M. Atzori, E. Berretti, A. Lavacchi, M. Fittipaldi, A. I. Chumakov, R. Rüffer, P. Rosa, M. Mannini, *ACS Appl. Mater. Interfaces* **2020**, *12*, 31696.
[16] R. Torres-Cavanillas, M. Morant-Giner, G. Escorcia-Ariza, J. Dugay, J. Canet-Ferrer, S. Tatay, S. Cardona-Serra, M. Giménez-Marqués, M. Galbiati, A. Forment-Aliaga, E. Coronado, *Nat. Chem.* **2021**, *13*, 1101.
[17] T. K. Ekanayaka, G. Hao, A. Mosey, A. S. Dale, X. Jiang, A. J. Yost, K. R. Sapkota, G. T. Wang, J. Zhang, A. T. N'Diaye, A. Marshall, R. Cheng, A. Naeemi, X. Xu, P. A. Dowben, *Magnetochemistry* **2021**, *7*, 37.
[18] M. D. Manrique-Juarez, S. Rat, F. Mathieu, D. Saya, I. Séguy, T. Leïchlé, L. Nicu, L. Salmon, G. Molnár, A. Bousseksou, *Appl. Phys. Lett.* **2016**, *109*, 061903.
[19] M. D. Manrique-Juarez, F. Mathieu, V. Shalabaeva, J. Cacheux, S. Rat, L. Nicu, T. Leïchlé, L. Salmon, G. Molnár, A. Bousseksou, *Angew Chem, Int Ed* **2017**, *56*, 8074.
[20] M. D. Manrique-Juárez, F. Mathieu, A. Laborde, S. Rat, V. Shalabaeva, P. Demont, O. Thomas, L. Salmon, T. Leichle, L. Nicu, G. Molnár, A. Bousseksou, *Adv. Funct. Mater.* **2018**, *28*, 1801970.
[21] M. Piedrahita-Bello, M. Piedrahita-Bello, J. E. Angulo-Cervera, J. E. Angulo-Cervera, R. Courson, G. Molnár, L. Malaquin, C. Thibault, B. Tondu, L. Salmon, A. Bousseksou, *J. Mater. Chem. C* **2020**, *8*, 6001.
[22] J. E. Angulo-Cervera, M. Piedrahita-Bello, B. Martin, E. Dantras, L. Nicu, T. Leichle, K. Dalla Francesca, A. da Costa, A. Ferri, R. Desfeux, L. Salmon, G. Molnár, A. Bousseksou, *J. Mater. Chem. C* **2022**, *10*, 8466.
[23] M. Piedrahita-Bello, Y. Zan, A. Enriquez-Cabrera, G. Molnár, B. Tondu, L. Salmon, A. Bousseksou, *Chem. Phys. Lett.* **2022**, *793*, 139438.
[24] K. Bairagi, O. Iasco, A. Bellec, A. Kartsev, D. Li, J. Lagoute, C. Chacon, Y. Girard, S. Rousset, F. Miserque, Y. J. Dappe, A. Smogunov, C. Barreteau, M. L. Boillot, T. Mallah, V. Repain, *Nat. Commun.* **2016**, *7*, 12212.
[25] L. Kipgen, M. Bernien, S. Ossinger, F. Nickel, A. J. Britton, L. M. Arruda, H. Naggert, C. Luo, C. Lotze, H. Ryll, F. Radu, E. Schierle, E. Weschke, F. Tuczek, W. Kuch, *Nat. Commun.* **2018**, *9*, 2984.
[26] L. Poggini, M. Milek, G. Londi, A. Naim, G. Poneti, L. Squillantini, A. Magnani, F. Totti, P. Rosa, M. M. Khusniyarov, M. Mannini, *Mater. Horiz.* **2018**, *5*, 506.
[27] M. Atzori, L. Poggini, L. Squillantini, B. Cortigiani, M. Gonidec, P. Bencok, R. Sessoli, M. Mannini, *J. Mater. Chem. C* **2018**, *6*, 8885.
[28] L. Kipgen, M. Bernien, F. Tuczek, W. Kuch, *Adv. Mat.* **2021**, *33*, 2105663.
[29] M. Gavara-Edo, R. Córdoba, F. J. Valverde-Muñoz, J. Herrero-Martín, J. A. Real, E. Coronado, *Adv. Mat.* **2022**, *34*, 2202551.
[30] M. Bernien, H. Naggert, L. M. Arruda, L. Kipgen, F. Nickel, J. Miguel, C. F. Hermanns, A. Kru, D. Kru, F. Tuczek, W. Kuch, *ACS Nano* **2015**, *9*, 8960.
[31] L. Poggini, G. Londi, M. Milek, A. Naim, V. Lanzilotto, B. Cortigiani, F. Bondino, E. Magnano, E. Otero, P. Sainctavit, M. A. Arrio, A. Juhin, M. Marchivie, M. M. Khusniyarov, F. Totti, P. Rosa, M. Mannini, *Nanoscale* **2019**, *11*, 20006.
[32] S. Johannsen, S. Ossinger, J. Grunwald, A. Herman, H. Wende, F. Tuczek, M. Gruber, R. Berndt, *Angew Chem, Int Ed* **2022**, *61*, e202115892.
[33] J. Liu, Y. Gao, T. Wang, Q. Xue, M. Hua, Y. Wang, L. Huang, N. Lin, *ACS Nano* **2020**, *14*, 11283.
[34] K. S. Kumar, M. Ruben, *Angew Chem, Int Ed* **2021**, *60*, 7502.
[35] E. J. Devid, P. N. Martinho, M. V. Kamalakar, I. Šalitroš, Ú. Prendergast, J. F. Dayen, V. Meded, T. Lemma, R. González-Prieto, F. Evers, T. E. Keyes, M. Ruben, B. Doudin, S. J. van der Molen, *ACS Nano* **2015**, *9*, 4496.
[36] A. Ulman, *Chem. Rev.* **1996**, *96*, 1533.
[37] L. Pukenas, F. Benn, E. Lovell, A. Santoro, L. J. Kershaw Cook, M. A. Halcrow, S. D. Evans, *J. Mater. Chem. C* **2015**, *3*, 7890.
[38] V. García-López, M. Palacios-Corella, V. Gironés-Pérez, C. Bartual-Murgui, J. A. Real, E. Pellegrin, J. Herrero-Martín, G. Aromí, M. Clemente-León, E. Coronado, *Inorg. Chem.* **2019**, *58*, 12199.
[39] N. Giaconi, A. L. Sorrentino, L. Poggini, G. Serrano, G. Cucinotta, E. Otero, D. Longo, H. Douib, F. Pointillart, A. Caneschi, R. Sessoli, M. Mannini, *Magnetochemistry* **2022**, *8*, 14.
[40] H. A. Goodwin, *Spin Crossover in Transition Metal Compounds II*, Springer, Berlin, Heidelberg, **2004**, pp. 23–47.
[41] S. Hayami, Y. Komatsu, T. Shimizu, H. Kamihata, Y. H. Lee, *Coord. Chem. Rev.* **2011**, *255*, 1981.
[42] S. Hayami, M. Nakaya, H. Ohmagari, A. S. Alao, M. Nakamura, R. Ohtani, R. Yamaguchi, T. Kuroda-Sowa, J. K. Clegg, *Dalton Trans.* **2015**, *44*, 9345.
[43] S. Hayami, K. Hashiguchi, G. Juhász, M. Ohba, H. Okawa, Y. Maeda, K. Kato, K. Osaka, M. Takata, K. Inoue, *Inorg. Chem.* **2004**, *43*, 4124.
[44] S. Hayami, Y. Shigeyoshi, M. Akita, K. Inoue, K. Kato, K. Osaka, M. Takata, R. Kawajiri, T. Mitani, Y. Maeda, *Angew Chem, Int Ed* **2005**, *44*, 4899.
[45] S. Hayami, N. Motokawa, A. Shuto, N. Masuhara, T. Someya, Y. Ogawa, K. Inoue, Y. Maeda, *Inorg. Chem.* **2007**, *46*, 1789.
[46] S. Hayami, K. Murata, D. Urakami, Y. Kojima, M. Akita, K. Inoue, *Chem. Commun.* **2008**, 6510.
[47] S. Hayami, K. Kato, Y. Komatsu, A. Fuyuhiro, M. Ohba, *Dalton Trans.* **2011**, *40*, 2167.

[48] R. Akiyoshi, Y. Komatsumaru, M. Donoshita, S. Dekura, Y. Yoshida, H. Kitagawa, Y. Kitagawa, L. F. Lindoy, S. Hayami, *Angew Chem, Int Ed* **2021**, *60*, 12717.
[49] M. Nakaya, W. Kosaka, H. Miyasaka, Y. Komatsumaru, S. Kawaguchi, K. Sugimoto, Y. Zhang, M. Nakamura, L. F. Lindoy, S. Hayami, *Angew Chem, Int Ed* **2020**, *59*, 10658.
[50] E. C. Constable, E. L. Dunphy, C. E. Housecroft, M. Neuburger, S. Schaffner, F. Schaper, S. R. Batten, *Dalton Trans.* **2007**, 4323.
[51] A. Krzykawska, J. Ossowski, T. Zaba, P. Cyganik, *Chem. Commun.* **2017**, *53*, 5748.
[52] H. Aitchison, R. Ortiz De La Morena, R. Peifer, S. Omar, H. Lu, S. M. Francis, M. Zharnikov, A. Grohmann, M. Buck, *Langmuir* **2018**, *34*, 9654.
[53] J. Yang, R. X. Hu, M. B. Zhang, *J. Solid State Chem.* **2012**, *196*, 398.
[54] A. Abhervé, M. Clemente-León, E. Coronado, C. J. Gómez-García, M. López-Jordà, *Dalton Trans.* **2014**, *43*, 9406.
[55] V. Garciá-López, M. Palacios-Corella, A. Abhervé, I. Pellicer-Carreño, C. Desplanches, M. Clemente-León, E. Coronado, *Dalton Trans.* **2018**, *47*, 16958.
[56] P. Totaro, L. Poggini, A. Favre, M. Mannini, P. Sainctavit, A. Cornia, A. Magnani, R. Sessoli, *Langmuir* **2014**, *30*, 8645.
[57] G. Poneti, L. Poggini, M. Mannini, B. Cortigiani, L. Sorace, E. Otero, P. Sainctavit, A. Magnani, R. Sessoli, A. Dei, *Chem. Sci.* **2015**, *6*, 2268.
[58] N. Giaconi, A. L. Sorrentino, L. Poggini, M. Lupi, V. Polewczyk, G. Vinai, P. Torelli, A. Magnani, R. Sessoli, S. Menichetti, L. Sorace, C. Viglianisi, M. Mannini, *Angew Chem, Int Ed* **2021**, *60*, 15276.
[59] S. Grimme, C. Bannwarth, P. Shushkov, *J. Chem. Theory Comput.* **2017**, *13*, 1989.
[60] C. Bannwarth, E. Caldeweyher, S. Ehlert, A. Hansen, P. Pracht, J. Seibert, S. Spicher, S. Grimme, *Wiley Interdiscip. Rev.: Comput. Mol. Sci.* **2021**, *11*, e1493.
[61] E. R. Johnson, S. Keinan, P. Mori-Sánchez, J. Contreras-García, A. J. Cohen, W. Yang, *J. Am. Chem. Soc.* **2010**, *132*, 6498.
[62] Z. Starowicz, R. Wojnarowska-Nowak, P. Ozga, E. M. Sheregii, *Colloid Polym. Sci.* **2018**, *296*, 1029.
[63] S. Luo, A. Mancini, F. Wang, J. Liu, S. A. Maier, J. C. de Mello, *ACS Nano* **2022**, *16*, 7438.
[64] N. F. L. Machado, M. P. M. Marques, L. A. E. Batista de Carvalho, J. L. Castro, J. C. Otero, *J. Raman Spectrosc.* **2017**, *48*, 413.
[65] C. K. Nandi, M. K. Hazra, T. Chakraborty, *J. Chem. Phys.* **2005**, *123*, 124310.
[66] A. Królikowska, J. Bukowska, *J. Raman Spectrosc.* **2007**, *38*, 936.
[67] J. Kožíšek, J. Svoboda, J. Zedník, B. Vlčková, I. Šloufová, *J. Phys. Chem. B* **2021**, *125*, 12847.
[68] M. G. Cowan, J. Olguín, S. Narayanaswamy, J. L. Tallon, S. Brooker, *J. Am. Chem. Soc.* **2012**, *134*, 2892.
[69] J. Ling, Y. Lu, L. Liu, X. Liu, L. Wang, *Phys. E* **2016**, *81*, 19.
[70] D. Jiang, Y. Lu, J. Ling, X. Leng, X. Liu, L. Wang, *Surf. Rev. Lett.* **2016**, *23*, 1650061.
[71] H. Aitchison, R. Ortiz De La Morena, R. Peifer, S. Omar, H. Lu, S. M. Francis, M. Zharnikov, A. Grohmann, M. Buck, *Langmuir* **2018**, *34*, 9654.
[72] I. Cebula, H. Lu, M. Zharnikov, M. Buck, *Chem. Sci.* **2013**, *4*, 4455.
[73] J. A. Barth, M. Rudolph, E. Uhlig, *Z. Anorg. Allg. Chem.* **1986**, *632*, 65.
[74] B. C. Beard, *Surf. Sci. Spectra* **1993**, *2*, 97.
[75] T. Ivanova, A. Naumkin, A. Sidorov, I. Eremenko, M. Kiskin, *J Electron Spectrosc. Relat. Phenom.* **2007**, *156–158*, 200.
[76] G. Poneti, M. Mannini, B. Cortigiani, L. Poggini, L. Sorace, E. Otero, P. Sainctavit, R. Sessoli, A. Dei, *Inorg. Chem.* **2013**, *52*, 11798.
[77] J. F. Moulder, W. F. Stickle, P. E. 'Sobol, K. D. Bomben, *Handbook of X-Ray Photoelectron Spectroscopy*, Perkin-Elmer Corp, Eden Prairie, MN, USA **1992**.
[78] D. Frost, C. Mcdowell, I. Woolsey, *Chem. Phys. Lett.* **1972**, *17*, 320.
[79] D. C. Frost, C. A. McDowell, I. S. Woolsey, *Mol. Phys.* **1974**, *27*, 1473.
[80] D. Briggs, V. A. Gibson, *Chem. Phys. Lett.* **1974**, *25*, 493.
[81] Y.u. G. Borod'ko, S. I. Vetchinkin, S. L. Zimont, I. N. Ivleva, Y.u. M. Shul'Ga, *Chem. Phys. Lett.* **1976**, *42*, 264.
[82] N. Bouldi, M. Mannini, M. Retegan, R. G. Miller, B. Cahier, P. Sainctavit, N. Guihéry, T. Mallah, D. Cabaret, D. Gouéré, F. Baudelet, L. Nataf, F. Wilhelm, F. Guillou, A. Rogalev, N. Suaud, S. Brooker, A. Juhin, *J. Phys. Chem. B* **2022**, *126*, 5784.
[83] P. S. Miedema, M. M. Van Schooneveld, R. Bogerd, T. C. R. Rocha, M. Hävecker, A. Knop-Gericke, F. M. F. De Groot, *J. Phys. Chem. C* **2011**, *115*, 25422.
[84] J. Li, N. Menguy, M. A. Arrio, P. Sainctavit, A. Juhin, Y. Wang, H. Chen, O. Bunau, E. Otero, P. Ohresser, Y. Pan, *J. R. Soc., Interface* **2016**, *13*, 20160355.
[85] C. Cartier Dit Moulin, F. Villain, A. Bleuzen, M. A. Arrio, P. Sainctavit, C. Lomenech, V. Escax, F. Baudelet, E. Dartyge, J. J. Gallet, M. Verdaguer, *J. Am. Chem. Soc.* **2000**, *122*, 6653.
[86] S. Yazdani, J. Phillips, T. K. Ekanayaka, R. Cheng, P. A. Dowben, *Molecules* **2023**, *28*, 3735.